Available online at www.sciencedirect.com

ScienceDirect

Procedia Engineering 10 (2011) 2873–2881

Engineering Procedia

ICM11

# Residual Stresses in TiC-based Cermets Measured by Indentation

Fjodor Sergejev[a,*], Eduard Kimmari[a], Mart Viljus[b]

[a]*Department of Materials Engineering, Ehitajate tee 5, Tallinn 19086, Estonia*
[b]*Centre for Materials Research, Ehitajate tee 5, Tallinn 19086, Estonia*

**Abstract**

The carbide composites are best known for their high hardness; evaluate bending strength and excessive, ceramic-like, brittleness. The titanium carbide based carbide composites (TiC-based cermets) are prospective candidates for tooling in sheet-metal forming (stamping) processes. The wear resistance (adhesive and functional) of some TiC-Fe/Ni cermets is better than that of hardmetals. Previous studies have shown that TiC carbide grains better absorb plastic deformation during cyclic loading (fatigue) and have lower fatigue sensitivity if compared to tungsten carbide grains in conventional hardmetal (WC-Co).

The core-rim (double-carbide) structure of the carbide grains is characteristic for TiC-based cermets. The effect of core-rim structure on the behavior of the cermets is poorly investigated. Such a structure is highly dependent on the production technology (powder metallurgy routes) as the difference between the coefficients of thermal expansion of components is obvious cause of high residual stresses appearing after sintering of pressed powder parts. Although, the thermal expansion coefficients of TiC-based cermets are lower than those of WC-based hardmetals.

The instrumented indentation technique is used to determine the scope of residual stresses in TiC-based cermets. The first steps are made for evaluation of the residual stresses proportions of the carbide and binder phases, core-rim structures in carbide composites.



*Keywords*: Nanoindentation; Residual stresses; Hardmetal; Cermet

## 1. Introduction

The use of indentation techniques for mechanical properties (hardness, fracture toughness) evaluation of brittle materials (metal matrix composites, ceramics, hardmetal, cermets etc.) are very popular because of ease of tests conduction, no need for precise and expensive specimen preparation, standard tools (indenters) and equipment are used of specified geometry, a lot of measurements can be conducted on relatively small testpieces and so on.

Those techniques are improved and supplemented by new analytical procedures to gain better understanding of abilities, restrictions and accuracy of indentation methods [1, 2]. The method for measuring hardness and elastic modulus by instrumented indentation techniques has widely been adopted and used in the characterization of mechanical behavior of materials at small scales. Its attractiveness stems largely from the fact that mechanical

* Corresponding author. Tel.: +372-620-3354; fax: +372-620-3196.
*E-mail address*: Fjodor.Sergejev@ttu.ee.


Selection and peer-review under responsibility of ICM11 doi:10.1016/j.proeng.2011.04.477

properties can be determined directly from indentation load and displacement measurements without the need to image the hardness impression [3]. The indentation size effect is investigated for application at nano-scale [4].

**Nomenclature**

| | |
|---|---|
| $a$ | radius of the contact |
| $c$ | depth of short plane crack |
| $E_{\mathbf{I}}$ | Young's modulus of the indenter |
| $E$ | Young's modulus of the material |
| $h$ | maximum indentation depth (displacement into the sample) |
| $h_c$ | contact depth of the indentation (displacement into the sample) |
| $h_f$ | final (plastic) depth of the indentation (displacement into the sample) |
| $h_s$ | the amount of sink-in (displacement into the sample) |
| $r$ | radial direction |
| $P$ | loading direction |
| $R$ | radius of ball indenter |
| $z$ | vertical direction |
| $\alpha$ | thermal expansion coefficient |
| $\beta$ | relative plastic zone size |
| $\varepsilon_R$ | representative strain |
| $\nu_{\mathbf{I}}$ | Poisson's ratio of the indenter |
| $\nu$ | Poisson's ratio of the material |
| $\sigma_{res}$ | residual stress |
| $\sigma_y$ | yield stress |

Instrumented indentation tests results have shown steep dependence on the load. The materials indentation hardness and indenter penetration depth are in linear dependences from indentation load [1-4]. The analyses of the stresses have also revealed same dependence of residual stresses on the indentation load during indentation [5].

The stress measured by instrumented indentation technique is the actual response of the material to the indentation, hard and stiff indenter penetration into the materials surface. The stress field generated by the indentation process is heterogeneous and leads to plastic deformation and damage in the vicinity of the tip. Using Hertz's theory, the spatial dependence of the stress components during indentation can be estimated by considering the elastic contact of a spherical indenter with a semi-infinite half space. For a Berkovich tip, the ratio between maximum indentation depth and contact radius is approximately $a \approx 3h$ (see Fig. 1a). The mechanical properties measured by nanoindentation, therefore, correspond to a semi-ellipsoidal volume extending to about nine times the employed indentation depth ($z \approx 3a \approx 9h$) in the vertical direction ($z$) and about seven times this same depth ($2r \approx 4/\sqrt{3}a \approx 7h$) in the radial direction ($r$), see Fig. 1b. During nanoindentation testing it is the convention to take the mean pressure as the nanohardness [6].

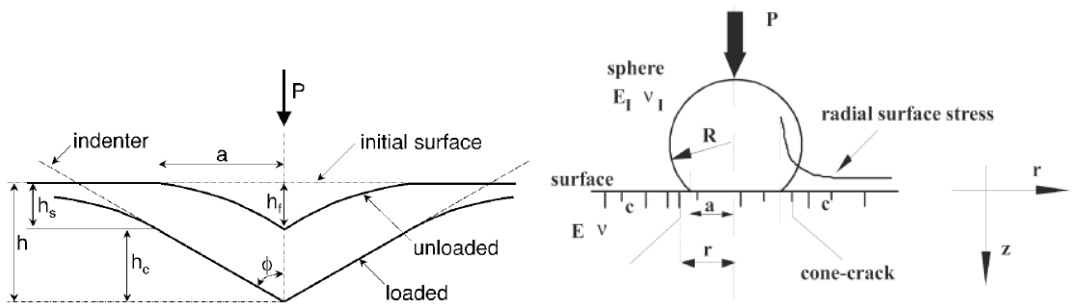


Fig. 1. Schematic illustration of: (a) the indentation showing parameters characterizing the contact geometry [3]; (b) Hertzian indentation [7]

Numerous studies are conducted to investigate the elastic-plastic indentation stress field employing the spherical indenters (Hertz's theory) as most reliable one, supported by finite-element (FE) methods [8, 9]. Only few of them are describing indentation behavior of hard materials [10].

The results of indentation hardness measurements performed on a range of brittle solids demonstrate that the indentation pressure is indenter shape insensitive over a wide range of geometries. Observations (and numerical calculations) indicate that the plastic zone exhibits spherical symmetry, regardless of indenter geometry and that identical plastic zone boundaries develop for spherical and Vickers pyramidal indentations of equal volume [5].

The residual stress from indentation is only the part of whole residual stress appearing in the vicinity of material structure due to the thermal expansion dismatch of the components. With increase of indentation load the response of the material, its ability to withstand indentation, increases as well and lead to the larger amount of the residual stress to resist the penetration of the indenter into material.

The first attempts to measure the residual stresses in brittle materials were taken many decades ago and all of them are implemented by comparison of stressed and stress-free specimens [11-13]. Recently the FE modeling method was proposed for determination of residual stresses from stressed specimen without need of comparison with stress-free material. This method is found to be reliable and applicable for brittle materials also [14-16].

Present study is the first step in measurement of the residual stresses of TiC-based (with Fe/Ni and Ni/Mo binders) cermets and separately carbide and binder phases. The conventional WC-15 wt%Co hardmetal was used as reference material for better comparison of testing results.

## 2. Experimental procedure

The nanoindentation technique, Micromaterials NanoTest system with use of Berkovich indenter (tip radius of about 100 nm), was used for indentation of studied materials. At least one hundred indentations were made for each load, ranging from 10 up to 500 mN. The step of indentation varied depending on load and was minimum of 3 μm for 10 mN and maximum of 30 μm for 500 mN load. Lower indentation loads (below 10 mN) were not used as it

became very difficult to make out the indents with diagonal size smaller than 0.5 μm, see Fig. 2 and 3. Another consideration was to use large enough loads to ensure sufficient plastic work of indentation component ($W_p$, area within load-displacement indentation curve) as the elastic component is high for carbide phase.

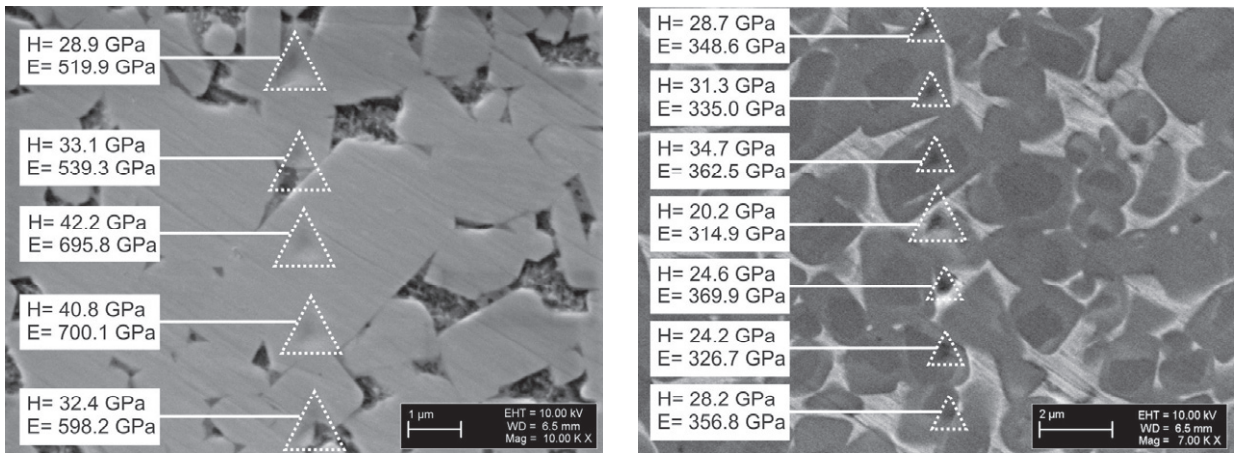


Fig. 2. SEM image of the nanoindentation imprints (with correspondent hardness and elastic modulus values): (a) on WC-15 wt% Co by 10 mN load; (b) on TiC-25 wt% Fe/Ni by 10 mN load.

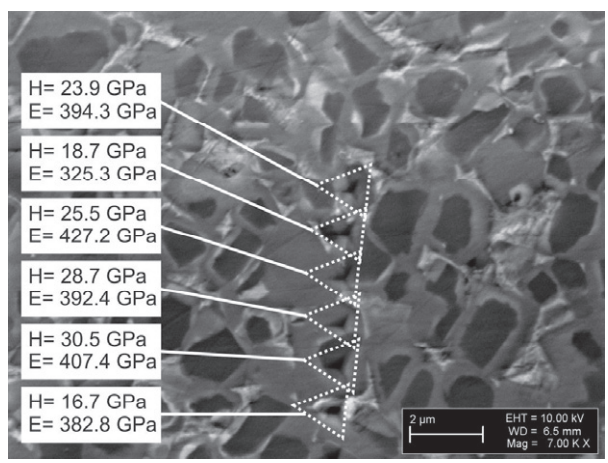


Fig. 3. SEM image of the nanoindentation imprints (with correspondent hardness and elastic modulus values) on TiC-30 wt% Ni/Mo by 10 mN load.

The indentation tests were complemented by scanning electron microscopy (SEM) and atomic force microscopy (AFM) studies of indents to verify the sizes of indents, measure the sink-in or pile-up and plastically deformed zone, and define carbide and binder phase indents. The scanning electron microscopes (Zeiss EVO MA15 and HITACHI TM-1000) and AFM.

### *2.1. Materials studied*

Two TiC-based cermets, one with iron-nickel and other with nickel-molybdenum binder, and conventional WC-Co hardmetal are investigated. The main mechanical properties along with composition and microstructural parameters can be found from Table 1. All materials were produced in Powder Metallurgy Laboratory at Tallinn

University of Technology. The testpieces were produced through conventional press and vacuum sinter (and sinter/HIP for ST75/14) powder metallurgy according to ASTM B406. Then specimens were prepared to following dimensions (width × height × length) - (15.0±0.3) × (5.0±0.3) ×35 mm$^3$.

Table 1. Composition, mechanical properties and microstructural parameters of carbide composites tested

| Grade | Composition and microstructure | | | Mechanical properties | | | | |
|---|---|---|---|---|---|---|---|---|
| | Carbide, wt% | Binder, wt% | Average carbide grain size $d_g$, μm | Transverse rupture strength $R_{TZ}$, MPa | Vickers hardness HV, MPa | Elastic modulus $E$, GPa | Fracture toughness $K_{IC}$, MPa·m$^{1/2}$ | Poisson ratio $v$ |
| H15 | WC, 85 | Co, 15 | 1.98 | 2900 | 1170 | 560 | 15.2 | 0.23 |
| ST75/14 | TiC, 75 | Fe/Ni, 25 | 2.03 | 2420 | 1400 | 420 | 14.3 | 0.30 |
| T30A | TiC, 70 | Ni/Mo, 30 | 2.00 | 1600 | 1280 | 395 | 16.9 | 0.31 |

Finally specimens were ground and polished on cloth with 1 μm diamond paste to a surface roughness of about $R_a$=0.2 μm on two sides (measured along 8 mm of the specimen by the Surtronic 3+ apparatus, using CR filter). Opposite ground faces were parallel within 0.03 mm. In order to remove surface contaminants, the samples were cleaned in alcohol and dried by compressed air.

### *2.2. Thermal residual stresses*

As the hardmetals and cermets are the carbide composite materials containing two very different phases, with different coefficients of thermal expansion (CTE), the mismatch in CTE between carbides and binders can be theoretically calculated. The powder metallurgy routes use high sintering temperatures, from 1280°C for cermets up to 1420°C for hardmetal. The thermal residual stress ($\sigma_{th}$) can be found from:

$$\sigma_{th} = \alpha E(T-Ts)/(1-\nu) \quad (1)$$

where α – is the thermal expansion coefficient, $10^{-6}$ °C;
E – Young's modulus, GPa;
T – is the shrinkage temperature, °C;
Ts – is the sintering temperature, °C;
ν – is the Poisson's ratio.

The largest thermal stress is calculated to appear in T30A cermet equal to compressive 1,66 GPa. The lowest thermal stress is found to be in H15 hardmetal (-1,29 GPa) and ST75/14 can contain residual thermal stress as high as 1,61 GPa. Depending on surface treatment and hardmetal composition the total compressive residual stress can reach -2.13 GPa [17]. For studied materials the values of calculated residual thermal stresses seems to be quit reasonable.

### *2.3. Analytical procedure*

The aim of the study was to find a simple yet precise enough procedure to obtain the residual stresses based on the results of indentations from single specimen, without need to comparison with stress-free specimen. The main idea is quit simple. There is a difference between values of the projected contact area ($A$) found from the fundamental relationship

$$H=P/A \quad (2)$$

and projected contact area ($A_c$) calculated using the indentation results by

$$Ac=24,56h_f^2 \quad (3)$$

We extract the representative strain ($\varepsilon_R$) from difference in the projected contact area values according to

$$\varepsilon_R=(A_c-A)/A \quad (4)$$

Ogasawara et al. (2005) showed that-absent residual stress-the optimum value of the representative strain for a Berkovich indenter is $\varepsilon_R$=0.0115. This value is a special case, valid for $\sigma_{res}$=0. If the representative strain approach is applicable to stressed specimens, we must now determine $\varepsilon_R$ ($\sigma_{res}$), i.e., determine how the representative strain varies with the residual stress.

The representative strain can only be determined numerically for each $\sigma_{res}$, since there is neither a direct physical meaning to $\varepsilon_R$, nor a closed form solution available from where the parameter can be extracted [16].

Plotting the test and calculation results on the plot with axes hardness ($H$) and representative strain ($\varepsilon_R$) we receive logarithmic dependence from which the optimum value can be found at the hardness equal to zero. Now the residual depths of the indentation can be found by substituting the optimum representative strain values into the equation (3), to calculate the residual projected contact areas. According to the received residual depths the residual hardness can be easily found from graphical dependences available for indentation tests , and then by exclusion of the residual hardness from experimentally received values the residual stress response to indentation can be found.

It was demonstrated by J. Yan et al. (2007) that the representative strain $\varepsilon_R$ is dependant from indenter shape, there is decrease of the strain values with increase of the indenter centerline-to-face angle, and almost independent from normalized residual stress ($\sigma_{res}$ / $\sigma_y$) [16]. As the dependence of the normalized residual stress from indenter shape is available the spherical cavity solution can be used for determination of the yield stress and residual stress values as follows

$$p / \sigma_y =2/3(1+ln(\beta)^3) \quad (5)$$

and

$$E / \sigma_y =3(1-v)(\beta^3)-2(1-2v) \quad (6)$$

where $p$ – is the indentation pressure;
$\beta$ – is the relative plastic zone size.

The relative plastic zone can be defined as the ratio of the plastic zone volume ($V$) and the indentation volume ($\Delta V$) or as the relation of plastic zone radius $b$ to indent contact radius $a$ as follows

$$\beta=b/a=(V/\Delta V)^{1/3} \quad (7)$$

The results of residual stresses calculations are shown in the table 2.

Table 2. Results of the residual stress analytical procedure for indentation at 10 mN

| Grade | Relative plastic zone $\beta$ | Yield stress $\sigma_y$, MPa | Residual stress $\sigma_{res}$, MPa |
|---|---|---|---|
| H15 | 7,67 | 710 | -425 |
| ST75/14 | 7,38 | 675 | -405 |
| T30A | 7,68 | 505 | -305 |

The plastic zone radius was measured by AFM from indents surfaces, see Fig. 4. The topography also showed the traces of plastic deformation around the indents, even for carbide grains, shown in Fig. 5.

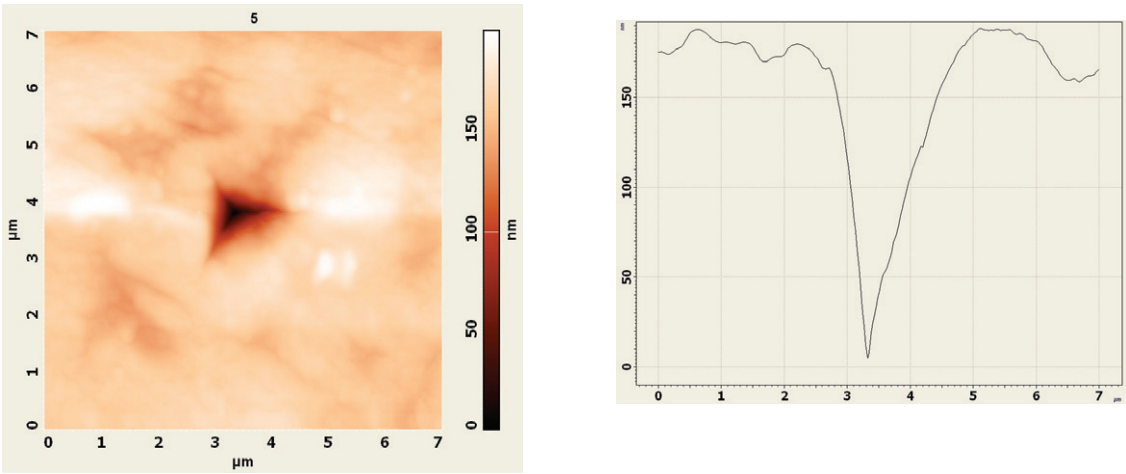


Fig. 4. (a) AFM image of indent on T30A at 10 mN load; (b) cross-section topography of same indent.

From Fig. 4b it can be seen that the plastically deformed zone size is quite large and at that particular case is around 2 µm wider than indent size. The height of the pile-up is about 30 nm, that's one fifth of the indent final (plastic) depth.

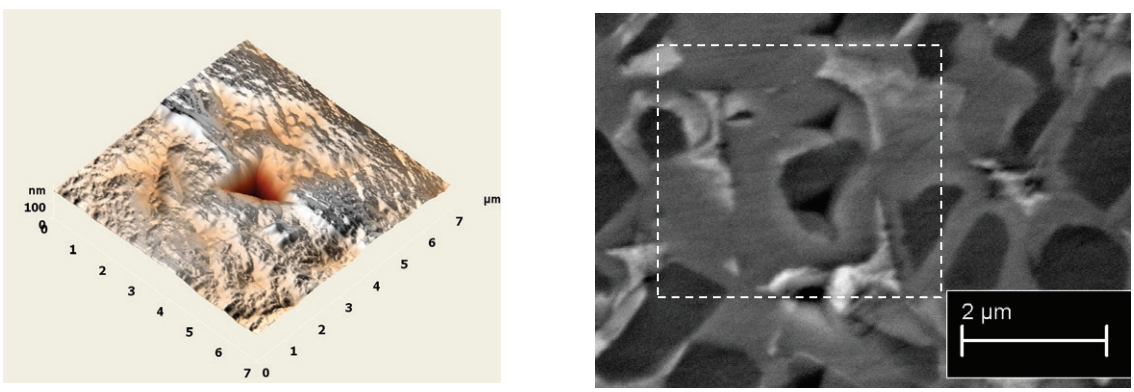


Fig. 5. (a) AFM 3D image from T30A cermet surface indented at 10 mN; (b) same indent on the SEM image (marked by dashed line).

On the 3D AFM topography it even can be seen that the indent is located in the centre of large TiC-carbide grain (Fig. 5a), and if compared with SEM from the same spot, it can be seen that the indent is in the core of the double carbide structure, see Fig. 5b.

The indentations at low loads (10 mN) allowed distinguishing the indents made on carbide grains and on binder.

## 3. Results and discussion

The results of the analytical procedure for residual stresses determination in the TiC-based cermets and WC-Co hardmetal as reference material have shown that this simple technique is applicable for brittle materials. Results approximation for indentations of higher loads, like Vickers 10, 30 and 50 kgf, are quite adequate and are 0.68-0.73 GPa compressive stress for H15, 0.64-0.70 GPa for ST75/14 and 0.66-0.71 GPa for T30A. As we can see the magnitude of the obtained residual stresses for all materials are in good agreement with theoretical values of the thermal stress calculated previously. The lower values of the residual stresses for nanoindentation can be justified by the fact of material response to indentation load. With increase of load the effect of residual stresses will be more

pronounced. Although it must be mentioned that we have not done any verifications of the residual stress values by more conventional methods like XRD or stress evaluation from FIB-SEM segments of the material. Those are the plans for future work.

The attempt to measure the residual stresses for every phase of the carbide separately have shown the relatively good results also. In case of separate WC and Co phases the difference is not only in magnitude (300-500 and 600 MPa, respectively) but also in stress type – compressive for WC and tensile for Co [18]. The residual stresses within WC particle are reported to distribute from high compression to tension [19]. We obtained the distribution of the residual stresses in the core-rim structures of the TiC-carbide grains (TiC-$Mo_2C$ for T30A cermet and TiC-$Fe_2C$ for ST75/14 cermet) from compression to tension, like it was previously shown for WC carbide. Unfortunately the distribution of the stresses is so wide that it is not possible to make any conclusions based on those results. The residual stresses varied from -0,53 to 0.74 GPa for WC grains and -0,5 to 0.6 GPa for TiC grains in both cermets. As it can be seen it is almost in same magnitude but of different type of stress. The distribution of the residual stresses for TiC-carbides is much complicated compared with tungsten carbides because of the core-rim structure (see Fig. 5b) and not yet understood composition of the rim in the carbide grains. The bordering areas can be seen between the core and rim structures there the composition can be quite different from both of core and the rim compositions due to diffusion processes during sintering and thermal treatment of powder materials.

The next step in the analysis of the residual stresses for different phases is the FE modeling technique application by procedure described in the [14-16]. We expect much more precisely obtained distribution of the stresses in the structures of carbide grains.

## 4. Conclusions

A simple analytical approach is used for residual stresses evaluation based on the results of the indentation tests at the nano scale (nanoindentation). Residual stresses can be calculated based on the assumption of the degree of the representative strain $\varepsilon_R$ arising during material testing (response of the material to indentation) dependence from residual stress $\sigma_{res}$. The residual stress calculation can be done by indentation results of only one specimen. There is no need for comparison with stress-free specimen as it is assumed for over residual stress determination methods. The main assumption of $\varepsilon_R$ of some value is characteristic to material at the stress free state ($\sigma_{res}$ =0) is used in calculation. Relatively large number of indentations at the different loads must be conducted to obtain more precise results.

The first attempts for evaluation of the residual stresses of the carbide and binder phases, core-rim structure in carbide composites are made. The distribution of the stresses varied from -0,53 to 0.74 GPa for WC grains (WC-15 wt%Co hardmetal) and -0,5 to 0.6 GPa for TiC grains in both cermets tested (TiC-Ni/Mo and TiC-Fe/Ni, with 30 and 30 wt% of binder respectively). Obtained stresses varied not only in magnitude but also in type of stress - from compressive to tensile, in both types of carbides investigated. No relations between stresses are found in dependence of carbide grain structure, due to complexity of core-rim structures and lack of reliable test data (nanoindentation results).

## Acknowledgements

This work was supported by the Estonian Ministry of Education and Research (project SF 0140062s08) and the Estonian Science Foundation (grant No. 7889). I am grateful to PhD Lauri Kollo and Dr. Jüri Pirso from Powder Metallurgy Laboratory of Tallinn University of Technology for providing the test materials and personal communications. PhD Valdek Mikli is also acknowledged for help in AFM analysis conduction and valuable discussions.

## References

[1] Oliver W. C., Pharr G. M. An improved technique for determining hardness and elastic modulus using load and displacement sensing indentation experiments. *J Mater Res* 1992; **7**: 1564-3.

[2] Ma D., Ong C. W., Zhang T. An instrumented indentation method for Young's modulus measurement with accuracy estimation. *Exp Mech* 2009; **49**: 719-9.

[3] Oliver W. C., Pharr G. M. Measurement of hardness and elastic modulus by instrumented indentation: Advances in understanding and refinements to methodology. *J Mater Res* 2004; **19**: 3-0.

[4] Huang Y., Feng X., Phar G. M., Hwang K. C. A nano-indentation model for spherical indenters. *Modelling Simul Mater Sci Eng* 2007; **15**: S255-2.

[5] Chiang S. S., Marshall D. B., Evans A. G. The response of solids to elastic/plastic indentation. I. Stresses and residual stresses. *J Appl Phys* 1982; **53**: 298-1.

[6] Bhushan B. *Springer handbook of nanotechnology*. 2nd ed. New York: Springer; 2007.

[7] Franco Jr. A., Roberts S. G. Surface mechanical analyses by Hertzian indentation. *Cerâmica* 2004; **50**: 94-8.

[8] Care G., Fischer-Cripps A. C. Elastic-plastic indentation stress fields using the finite-element method. *J Mater Sci* 1997; **32**: 5653-9.

[9] Herbert E. G., Pharr G. M., Oliver W. C., Lucas B. N., Hay J. L. On the measurement of stress-strain curves by spherical indentation. *Thin Solid Films* 2001; **398-399**: 331-5.

[10] Armstrong R. W., Ferranti Jr. L., Thadhani N. N. Elastic/plastic/cracking indentation behavior of hard materials. *Int J Refract Met H* 2006; **24**: 11-6.

[11] Roberts S. G., Lawrence C. W., Bisrat Y. Determination of surface residual stresses in brittle materials by Hertzian indentation: Theory and experiment. *J Am Ceram Soc* 1999; **82**: 1809-6.

[12] Bisrat Y., Roberts S. G. Residual stress measurement by Hertzian indentation. *Mater Sci Eng A* 2000; **288**: 148-3.

[13] Jang J. Estimation of residual stress by instrumented indentation: A review. *J Ceram Process Res* 2009; **10**: 391 0.

[14] Chen X., Yan J., Karlsson A. M. On the determination of residual stress and mechanical properties by indentation. *Mat Sci Eng A-Struct* 2006; **416**: 139-9.

[15] Zhao M., Chen X., Yan J., Karlsson A. M. Determination of uniaxial residul stress and mechanical properties by instrumented indentation. *Acta Mater* 2006; **54**: 2823-2.

[16] Yan J., Karlsson A. M., Chen X. Determining plastic properties of a material with residual stress by using conical indentation. *Int J Solids Struct* 2007; **44**: 3720-7.

[17] Miyano M., Hirose Y. *Advances in X-Ray Analysis*. New York: Plenum Press; 1997.

[18] Larsson C., Oden M. X-ray diffraction of residual stresses in functionally graded WC-Co composites. *Int J Refract Met H* 2004; **22**: 177-4.

[19] Seol K. Effects of WC size and amount on the thermal residual stress in WC–Ni composites. *Mat Sci Eng A-Struct* 2005; **398**: 15–1.